Colors of Ag^+-Exchanged Zeolite A

Roland Seifert, Ruedi Rytz, and Gion Calzaferri*

Department of Chemistry and Biochemistry, University of Berne, Freiestrasse 3, CH-3000 Bern 9, Switzerland

Received: March 8, 2000; In Final Form: June 1, 2000

UV/vis spectra of hydrated and activated $Ag^+_xNa^+_{12-x}A$, $Ag^+_xCa^{2+}_{6-0.5x}A$, and $Ag^+_{9.5}ZK$-4 materials were studied. Any absorption band or color observed in silver zeolite A materials is due to the presence of silver ions. The marked site preference of ions in $Ag^+_xCa^{2+}_{6-0.5x}A$ was found to offer the unique possibility of investigating different coordination sites of Ag^+ ions in zeolite A. Observations we made lead to the result that Ag^+ coordinated to 6- and 8-ring oxygens gives rise to electronic transitions in the near-UV region. Only Ag^+ coordinated to 4-ring oxygens leads to the 22 000 cm^{-1} absorption responsible for the typical deep yellow color. The red color which is caused by a strong absorption band at 19 000 cm^{-1} is observed if a 4-ring coordinated Ag^+ has a second Ag^+ as a neighbor. We assume that the second Ag^+ is at a 6-ring site. Yellow and red colored materials turn colorless again when exposed to humidity. The reversibility is complete for the yellow samples while a broad but weak absorption in the near-UV remains after rehydration of the red samples. Molecular orbital calculations were carried out on a unit structure cell consisting of 1296 atoms. The occupied frontier orbital region consists mainly of two bunches of levels: the HOMO region which spreads from about −11 to − 12.6 eV and the next lower lying levels below −13.6 eV. The HOMO region consists of oxygen lone pairs O(n). We find that 6-ring coordinated Ag^+ gives rise to near-UV electronic transitions and 4-ring coordinated Ag^+ causes a band in the visible. These transitions can be interpreted as charge transfer from zeolite oxygen lone pairs to Ag^+. We therefore denote them as $Ag^+(5s) \leftarrow O(n)$ LMCT.

1. Introduction

Rálek et al. reported in 1962 that hydrated colorless zeolite $Ag^+_xNa^+_{12-x}A$ turns yellow to brick-red on activation.[1] No explanation of this phenomenon was given at that time. Later it was believed that the color change was due to formation of silver clusters (Ag_n^0) in the cavities of silver zeolite A. These neutral silver species were assumed to form at elevated temperatures via an autoreduction process in which O_2 from the zeolite framework was released.[2] We recently showed that activation at room temperature under high vacuum is already sufficient to produce the yellow form of $Ag^+_xNa^+_{12-x}A$. The fully reversible color change which depends on the hydration state of the silver zeolite was attributed to electronic charge transfer transitions from the oxygen lone pairs of the zeolite framework to the empty 5s orbital of the Ag^+ ions, denoted as $Ag^+(5s) \leftarrow O(n)$.[3] Pure sodium ($Na^+_{12}A$) and calcium zeolite A (Ca^{2+}_6A) are colorless in both their hydrated and their activated (dehydrated) states. Silver-containing sodium zeolite A is colorless in its fully hydrated form. In activated silver zeolite A materials, the Ag^+ is forced to coordinate zeolite oxygen because an insufficient number of water molecules are available. The question remained if specific coordination sites which act as yellow and/or red "color centers" can be identified. We answer this question by studying the UV/vis spectra of $Ag^+_xNa^+_{12-x}A$ and of $Ag^+_xCa^{2+}_{6-0.5x}A$ materials upon room temperature and elevated temperature activation. We show that the marked site preference of ions in $Ag^+_xCa^{2+}_{6-0.5x}A$, which can be probed by gas adsorption experiments, offers the unique possibility of investigating properties of different Ag^+ coordination sites.

From our previous studies we have good reasons to assume that LMCT transitions in which electron density is transferred from zeolite oxygen to the silver cations contribute strongly to the UV/vis spectra of any silver zeolite A material. The α-cage used in the computational part of these studies, however, was too small to make the distinction between different positions as color centers possible.[3] This technical problem has been solved by using a zeolite unit consisting of 1296 atoms and we can now address the following questions: What is the nature of the HOMO and of the LUMO region? Which zeolite framework atoms contribute to an electronic transition? What is the influence of the local symmetry of the Ag^+ at 4- and at 6-ring sites? How important are Ag^+-Ag^+ interactions? This interplay between the experimental observations and the theoretical results leads to an advanced understanding of the interesting properties of silver zeolite A materials.

2. General

Description of the Structure. In the classical sense, zeolites are a class of crystalline aluminosilicates based on anionic frameworks with crystallographically well-defined channels and cavities. The primary building units are $[SiO_4]^{4-}$ and $[AlO_4]^{5-}$ tetrahedra linked together by corner-sharing, forming bent oxygen bridges.[4] Three-dimensional networks assembled of corner-sharing silicon−oxygen tetrahedra are electrically neutral. The presence of Al^{3+} induces an electrical imbalance leading to a negatively charged framework. In order to preserve the overall electrical neutrality, zeolites contain additional cations (one positive charge for each $[AlO_4]^{5-}$ unit). In an aqueous environment, these cations can undergo exchange reactions with cations of a surrounding solution. This property makes them widespread water softeners. Under ambient conditions the channels and cavities of zeolites are filled with water. This water

* Corresponding author. E-mail: gion.calzaferri@iac.unibe.ch.

10.1021/jp000905z CCC: $19.00
Published on Web 07/21/2000

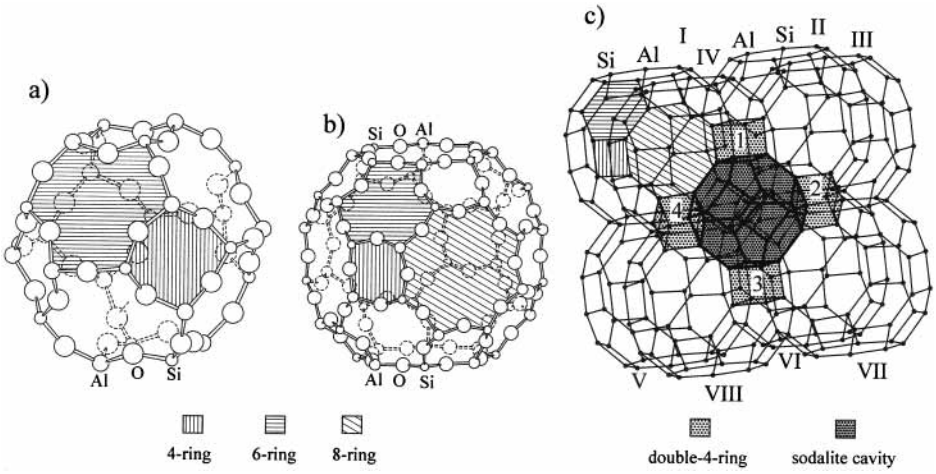

Figure 1. Representation of the structure of zeolite A: (a) β-cage (or sodalite cage), (b) α-cage, (c) unit structure cell (oxygen not shown),

can be removed under vacuum at elevated temperature without changing the structure of the framework. Anhydrous, so-called activated, zeolites have a high affinity for water which makes them efficient drying agents. Activated zeolites adsorb not only water but also size-selective neutral molecules. The abundance of different sizes and shapes of the channels and cavities of different types of zeolite has been exploited by employing them as molecular sieves in industrial separation processes. The inner surface of the zeolite can act as a catalyst, a property widely used in petrochemistry. Some 40 naturally occurring zeolites have been characterized and more than 3 times this number has been synthesized.[5] A prominent representative is zeolite A (Linde Type A) which was first prepared by Breck et al. in 1956.[6,7] In its sodium form the ideal sum formula is Na_{12}-$[(AlO_2)_{12}(SiO_2)_{12}]\cdot 27H_2O$. Zeolite A consists of an equal number of $[SiO_4]^{4-}$ and $[AlO_4]^{5-}$ tetrahedra. Other materials with the same structure but higher Si content are known under the name ZK-4.[8] According to the rule of Loewenstein, no neighboring aluminum tetrahedra are allowed to be present within the framework, leading to an alternation of silicon and aluminum tetrahedra in Zeolite A.[9] Basic features of the inner surface of the zeolite are *n*-rings, where *n* represents the number of oxygen atoms in the ring. The structure in Figure 1a is composed of 4-rings (vertical hatching) and 6-rings (horizontal hatching). It is differently referred to as a truncated octahedron, sodalite cavity, pseudo unit cell, or as β-cage. Elemental composition of zeolite A is usually given for this pseudo unit cell which consits of 24 tetrahedra. It is frequently used to describe zeolite A in terms of an assemblage of β-cages octahedrally joined at 4-rings by four bridging oxygens. The structure composed of 4-, 6-, and 8-rings depicted in Figure 1b consists of 48 tetrahedra. It is occasionally called truncated cuboctahedron or α-cage. Fusing eight α-cages (I, II, ..., VIII) at 8-rings leads to the unit cell of zeolite A shown in Figure 1c. In drawings of zeolite structures it is customary to drop the oxygen atoms and think of them as placed near the middle of lines joining neighboring silicon and aluminum atoms. Note that silicon and aluminum positions of neighboring β-cages are interchanged. Two secondary building units become apparent. In the center we can distinguish a sodalite cavity (dark shaded) and six double 4-rings, four of which are numbered as 1, 2, 3, and 4.

Exchangeable Ions. While the anionic framework is held together by covalent bonds, the exchangeable cations interact ionically within the framework. In the hydrated state these ions are coordinated by the framework and water or they are completely hydrated. In the activated state all cations are forced on coordination sites of the framework which are *n*-rings. They prefer rings with an aperture fitting their size. Due to their limited number, they may also occupy less favorable sites. Ions like Na^+, K^+, Ag^+, and Ca^{2+} that are not too big are expected to prefer 6-rings as coordination sites. Per pseudo unit cell, 12 negative charges must be compensated. Eight 6-rings, three 8-rings, and 18 4-rings are present to coordinate the cations. In the calcium form (Linde 5A) all six doubly charged cations are coordinated to 6-rings.[10] In the activated sodium form (Linde 4A), eight Na^+ are at 6-rings, three at the less favorable 8-rings, and one is forced into a 4-ring position located in the α-cage.[11] In mixed Ca^{2+}/Na^+-A one can observe the preference of the sodium ions to coordinate 6-rings. In $Na^+{}_4Ca^{2+}{}_4A$ (often also called Linde 5A) the 8- and 4-rings stay free, because all eight cations can find a 6-ring position. Crystallographic data indicate that 4-ring positions are only populated in the presence of 12 cations per pseudo unit cell.[12]

The distribution of the cations influences the adsorption properties of zeolite A, since all adsorption processes take place by diffusion through the 8-rings which have a free aperture of 5 Å, where the name Linde 5A comes from. Species with a kinetic diameter of more than 5 Å are excluded.[13] This maximum diameter is reduced by cations located at 8-ring positions. In the sodium form species exceeding 4 Å are excluded at room temperature. The different adsorption behavior is more pronounced at low temperatures. While $Ca^{2+}{}_6A$ readily adsorbs nitrogen at 77 K the sodium form does not. In the mixed Ca^{2+}/Na^+ form a sharp jump in the rate of diffusion can be observed when the total number of cations is about 10.[14] One 8-ring and all 4-ring positions are not populated if the total number of cations per pseudo unit cell is less or equal to 10. This gives rise to two unoccupied 8-ring positions per α-cage and therefore free access to the total inner surface.

Molecular Orbital Calculations. MO calculations were carried out on the zeolite unit illustrated in Figure 1c which consists of 1296 atoms with 4240 valence atomic orbitals (AOs), including 8 Ag^+. Given this size, there are not many computational methods available to study the HOMO/LUMO orbital region and to calculate the oscillator strength of the first electronic transitions. One of them is the EHMO-EDiT (EHMO = extended Hückel molecular orbital; EDiT = electronic dipole-induced transitions) method which was shown to be a powerful tool to investigate electronic dipole transitions in molecules, complexes, clusters,[15,16] and solids.[17] This was the method used.

Interaction between light and matter is the interaction between electric fields $\mathbf{E}(t)$, which vary in time, and charge distributions composed of nuclei and electrons. The area in which light is either absorbed or emitted is small compared to the dimension

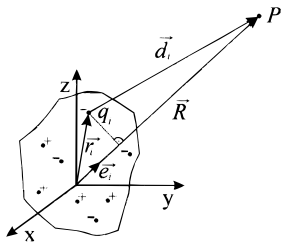

Figure 2. Electrostatic potential of a region probed by an observer P at distance R.

of the electric field which is of the order of the wavelengths of UV/vis radiation ($\approx 10^3$ Å). This is obvious for molecules, but roughly holds for the color centers we have investigated as well. Thus we wonder how any charge distribution which we choose to describe by its electrostatic potential ϕ looks like for a remote observer at *P* (Figure 2). If a point charge q_i causes a potential of $\phi_i(d_i) = 1/4\pi\epsilon_0(q_i/d_i)$ at *P*, the overall potential is given by summing up the single contributions:[18]

$$\phi = \sum_i \phi_i(d_i) = \frac{1}{4\pi\epsilon_0}\sum_i \frac{q_i}{d_i} \tag{1}$$

As we require the distance r_i between the point charge q_i and the center of the coordinate system to be much shorter than the distance *R* between the center of the coordinate system and the observer at *P*, we may approximate d_i by its projection onto *R*

$$d_i \approx R - \vec{r}_i \cdot \vec{e}_r = R - r_i e_r \cos a \tag{2}$$

where $\vec{e}_r$ is a unit vector pointing along $\vec{R}$. To prepare for insertion into eq 1, we formulate

$$\frac{1}{d_i} = \frac{1}{R - \vec{r}_i \cdot \vec{e}_r} = \frac{1}{R}\left[\frac{1}{1 - \frac{\vec{r}_i \cdot \vec{e}_r}{R}}\right] \tag{3}$$

Expanding the expression in brackets in a power series and cutting off after the first term yields

$$\frac{1}{d_i} \approx \frac{1}{R}\left[1 + \frac{\vec{r}_i \cdot \vec{e}_r}{R}\right] \tag{4}$$

which we now insert in eq 1 to give

$$\phi(R) \approx \frac{1}{4\pi\epsilon_0}\left[\frac{Q}{R} + \sum_i \frac{q_i \vec{r}_i \cdot \vec{e}_r}{R^2}\right] \tag{5}$$

Q is the total charge of the charge distribution under consideration. For the neutral objects investigated *Q* is zero. With the *dipole moment of the charge distribution* $\vec{\mu} = \sum_i q_i \vec{r}_i$, we finally obtain

$$\phi(R) \approx \frac{1}{4\pi\epsilon_0}\frac{\vec{\mu} \cdot \vec{e}_r}{R^2} \tag{6}$$

Thus, to a first approximation, we may think of the interaction between light and the color centers in terms of varying electric fields which induce the oscillation of an electric dipole, i.e., a nucleus to which an electron is attached. The nucleus is much heavier than the electron and therefore does not significantly contribute to the dipole oscillation. Its position may in fact be thought of as fixed. Thus, we are left with the electron moving through space upon excitation. In quantum theory, the path this electron travels is given by the *transition dipole length* D_{nm} defined as

$$D_{nm} = \langle \psi_n | \vec{r} | \psi_m \rangle \tag{7}$$

where $\vec{r}$ is the position operator of the electron undergoing the transition and Ψ_m and Ψ_n are the initial and final wave functions, respectively. D_{nm} is not an experimentally accessible quantity. However, its absolute value squared is. This takes us to the oscillator strength[15]

$$f_{ed} = l_0 \tilde{\nu} |D_{nm}|^2 \tag{8}$$

where l_0 is equal to 1.085×10^{-5} cm/Å^2 and $\tilde{\nu}$ is the energy in wavenumbers (cm^{-1}) of the transition $n \leftarrow m$. The relation between the molar decadic extinction coefficient ϵ and the oscillator strength f_{ed} can be expressed as follows

$$f_{ed} = 4.32 \times 10^{-9} \int_{band} \epsilon(\tilde{\nu})\, d\tilde{\nu} \tag{9}$$

Thus, the area under an absorption band is proportional to the oscillator strength of the transition. Typical values for electronic dipole-allowed transitions are in the range of $10^{-3}-1$.

3. Experimental Section

Synthesis of the Zeolites. Chemically pure and highly crystalline zeolite A was prepared and characterized as described in ref 19. Zeolite ZK-4 was synthesized following a procedure described by Kerr, which was modified for the use of chemically pure and completely soluble Al- and Si-sources.[8]

Synthesis of the Si Precursor. To obtain a readily soluble Si precursor for the synthesis of zeolite ZK-4, a solution of 72.86 g of diisopropylamine (Merck) in 75 mL of water was prepared in a round-bottom flask and cooled to room temperature. 150 g of tetraethyl orthosilicate ($Si(OEt)_4$, Aldrich, >99%) was slowly added under agitation to the solution and stirred for 48 h. The initially formed gel slowly changed into a white precipitate, which was separated by centrifugation. The solid was suspended several times in 400 mL of ethanol to obtain an almost odor-free product. To avoid its dusting, the precursor was dried first at room temperature under slightly reduced pressure, and later up to 100 °C in a vacuum over a period of 2−3 d. The ignition loss of the product was determined at 800 °C to 14%.

Synthesis of Zeolite ZK-4. Two solutions (A and B) were separately prepared under inert atmosphere in Teflon vessels. (A) 4.206 g of Si precursor ($SiO_2 \cdot H_2O$) was dissolved in an agitated solution of 25.74 g of teramethylamonium hydroxide pentahydrate (TMA, $(CH_3)_4NOH \cdot 5H_2O$, Aldrich, >99%) and 57 mL of H_2O at 90 °C. (B) 0.962 g of aluminum (Al, wire, d = 1 mm, Balzers, 99.999%) was dissolved in a solution of 2.108 g of NaOH (Fluka, >98%, p.a.) and 6.435 g of TMA in 50 mL of H_2O under agitation at 90 °C. The two clear solutions (A and B) were combined rapidly after cooling them to room temperature under vigorous stirring. The colloidal solution was agitated for 15 min at room temperature and then refluxed for 24 h. The white precipitate was separated and suspended three times in hot water. The supernatant was decanted every time after sedimentation of the product. The solid was dried at 80 °C. Tetramethylammonium ions were removed by calcination at 550 °C in air. The remaining protons were exchanged by suspending the product in 0.1 M $NaNO_3$ solution. Elemental composition was determined by EDX to $Na_{9.5}(Al_2O_3)_{4.75}(SiO_2)_{14.5}$.

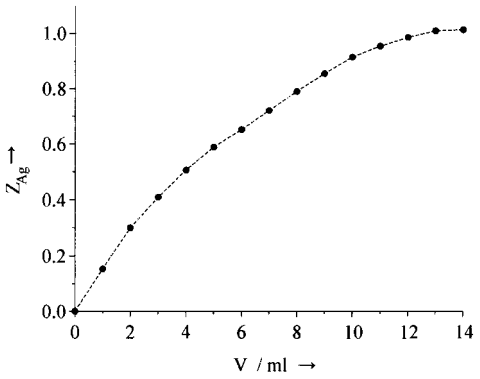

Figure 3. Titration curve of $Ca^{2+}{}_6A$ with $AgNO_3$. Z_{ag} is the exchange degree (silver content of the zeolite, $Z_{ag} = 1$ corresponds to 100% ≅ $Ag^{+}{}_{12}A$), V = volume of 0.1 N $AgNO_3$ solution added to a suspension of 100 mg of $Ca^{2+}{}_6A{\cdot}30H_2O$ in 100 mL of 0.02 N $Ca(NO_3)_2$ solution. Time for equilibration: 1−1.5 h.

Ion Exchange. For the UV−vis investigations, 80 mg of zeolite was always freshly exchanged with 0.1 M $AgNO_3$ (Merck Titrisol). Samples with exchange rates of up to 6 Ag^+ were prepared by suspending the zeolite in 5 mLof water and an appropriate amount of $AgNO_3$ for 15 min. Quantitative uptake of the Ag^+ ions can be assumed.[20,21] Subsequently, the zeolite was washed twice with water. Kept at 92% humidity, $Ag^{+}{}_xNa^{+}{}_{12-x}A$ was expected to have incorporated 27 H_2O molecules per formula unit.[13] In order to obtain fully Ag^+-exchanged samples, the zeolite was twice suspended for 15 min in 20 mL of $AgNO_3$ solution and thereafter washed three times with 15 mL of water.

$Ca^{2+}{}_6A$ was obtained by ion exchange from $Na^{+}{}_{12}A$ by suspending the zeolite three times in a 2-fold excess of 0.1 M aqueous $Ca(NO_3)_2$ solution for 1 h at room temperature. Mixed Ag^+/Ca^{2+} materials where obtained by adding a chosen quantity of 0.1 M $AgNO_3$, deduced from the exchange isotherm given in Figure 3, to a suspension of 100 mg of hydrated $Ca^{2+}{}_6A$ in 100 mL of 0.1 M $Ca(NO_3)_2$ for 1.5 h at 25 °C. The isotherm was obtained in a stepwise titration procedure, detecting the free Ag^+ in solution by a calibrated silver sensitive electrode under the same conditions. The samples were washed as described above.

Sample Preparation. 80−100 mg of exchanged zeolite was suspended in 2 mL of water and transferred into a quartz ampule (cylinder with a height of 2 cm and a radius of 0.75 cm) which had previously been connected to an HV-flange adapter so it was gastight. The ampule was thereafter horizontally connected to the pump, which allowed for an even deposition of the zeolite at the ampule's bottom. The extra water was evaporated at 10 mbar (2−3 h). For activation, the turbo pump (Alcatel) was connected until the final pressure of 10^{-7} mbar was reached after 48−72 h. After activation at room temperature, elevated temperature activation was performed by gradually heating to the desired temperature (±5 °C) with an adjustable heat pistol. The heating rate was chosen such that the pressure in the apparatus never exceeded 5×10^{-6} mbar, in order to avoid irreversible brown color changes. Ampules containing samples with sufficient adherence to the bottom were disconnected from the pump with a burner under gastight conditions and transferred into the spectrometer.

Physical Measurement. UV/vis spectra were recorded as diffuse reflection spectra with an Perkin-Elmer Lambda 14 spectrometer, equipped with an integrating sphere (Labsphere RSA-PE-20). Prior to plotting, the automatically collected data were converted using the Kubelka−Munk formula. Gas adsorption experiments were performed with a Sorptomatic 1990 (CE-Instruments). 0.3−0.4 g of sample was activated 12 h at room temperature, followed by a thermal activation up to 350 °C with a rate of 0.1 °C/min in HV (final pressure $<10^{-4}$ mbar). This temperature was held at least for 15 h. Argon was dosed stepwise to the sample which was cooled with liquid argon. In the low-pressure region ($p/p_0 < 0.015$), equilibrium was assumed when within 7 min the pressure over the sample did not change more than 0.005 mbar.

TABLE 1: Coulomb Integrals and Slater Exponents for EHMO-EDiT Calculations.

element	AO	H_{ii}/eV	ζ_1	ζ_2	c_1	c_2
Ag	5s	−12.13	1.850			
	5p	−4.17	1.300			
	4d	−18.76	3.912	1.545	0.8242	0.3291
Al	3s	−16.77	1.500			
	3p	−10.41	1.500			
Si	3s	−21.79	1.700			
	3p	−13.52	1.700			
O	2s	−26.68	2.575			
	2p	−11.25	2.275			
O[a]	2s	−26.81	2.575			
	2p	−11.36	2.275			
H	1s	−16.06	1.300			

[a] Refer to oxygen atoms of the OH groups.

Calculations. Extended Hückel molecular orbital calculations[22] were carried out with the ICON-EDiT program package.[23] The off-diagonal elements were approximated as[24]

$$H_{ij} = 1/2kS_{ij}(H_{ii} + H_{jj}) \tag{10}$$

using the weighted Wolfsberg−Helmholz formula[25] in its distance-dependent form[26]

$$k = 1 + [\kappa + \Delta^2 - \Delta^4\kappa]\left[\frac{e^{-\delta(R-d_0)}}{1 + \{\delta(R - d_0 - |R - d_0|)\}^2}\right] \tag{11}$$

$$\Delta = \left(\frac{H_{ii} - H_{jj}}{H_{ii} + H_{jj}}\right) \tag{12}$$

Equations 10−12 are the defaults implemented in ICON-EDiT. Standard κ and δ values of 1.0 and 0.35 Å^{-1}, respectively, were applied. H_{ii} and H_{jj} are the Coulomb parameters of the ith and jth atomic orbital. They were determined by means of an SCCC (self-consistent charge configuration) procedure[27,28] with parameters given elsewhere.[16,23] In order to reduce the computational burden, the charge iteration was carried out on an α-cage, whose dangling bonds were saturated with OH groups. The silver atom was placed at the center of a 6-ring. Oxygen atoms of the zeolite framework and of the saturating OH groups had to be distinguished; see also ref 3. The resulting Coulomb integrals along with the Slater parameters are listed in Table 1. All other calculations, however, were carried out on the complete system reported in Figure 1c.

The worked out extended Hückel wave functions and respective energies were subsequently employed to compute the oscillator strengths as well as the density of levels (DOL) and the density of transitions (DOT). Our treatment basically relies on a procedure described elsewhere.[28] However, for the sake of an easier and generally valid programming some effort was necessary to adjust the procedure.[15,23,29]

We make use of the terms DOL and DOT. The density of levels (DOL) counts the number of energy levels (molecular orbitals) in a given (small) energy range. In its limiting case

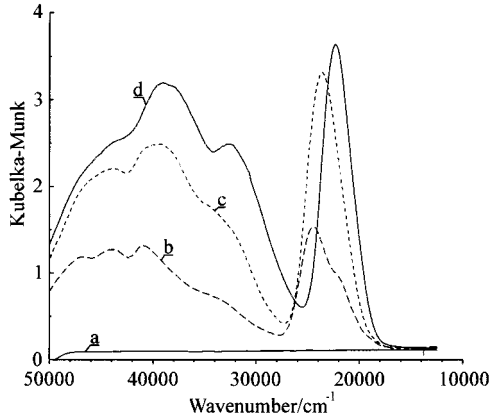

Figure 4. UV/vis spectra of $Ag^+_xNa^+_{12-x}A$, activated at room temperature: (a) $x = 0$; (b) $x = 0.5$; (c) $x = 1$; (d) $x = 6$.

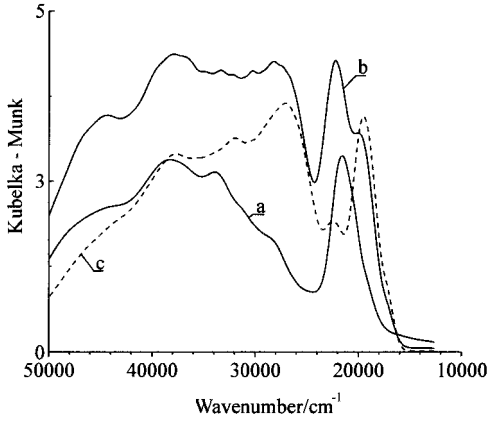

Figure 5. UV/vis spectra of $Ag^+_xNa^+_{12-x}A$, activated up to 200 °C: (a) $x = 1$; (b) $x = 6$; (c) $x = 12$.

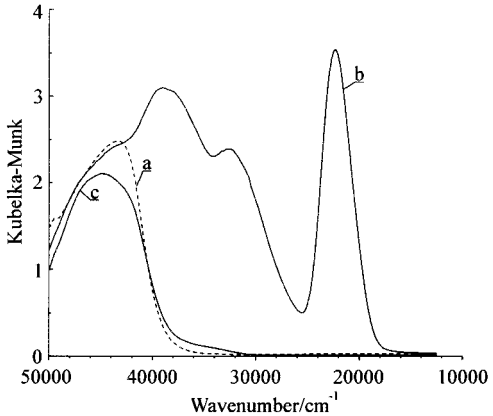

Figure 6. UV/vis spectra of $Ag^+_6Na^+_6A$: (a) freshly exchanged, never activated; (b) activated at room temperature; (c) activated at room temperature and exposed to pure water vapor before measurement.

for very large systems, it is identical to the density of states (DOS) well-known from solid state chemistry.[30] The density of transitions (DOT) is closely related to the DOL in the sense that it counts the number of transitions in a given energy region. It may therefore be regarded as a joint density of levels of initial and final wave functions.

For the actual computation of the oscillator strengths we start from EHMO wave functions written as products of one-electron molecular orbitals. It can be shown that the computation of the f_{ed} values can be restricted to the two MOs which change their occupation on excitation.[28] If we denote the initial and final MOs with Ψ_i and Ψ_f, respectively, we find the oscillator strength to be proportional to the energy difference of the contributing MOs, $\tilde{\nu}$, and to the $|D_{fi}|^2$. The factor l_0, however, has to be doubled if Ψ_i is occupied by two electrons.[31] Working out the transition-dipole length D_{fi} is quite a chore and involves the computation of an $n \times n$ matrix where n is the number of AOs constituting the MO. The matrix form of D_{fi} is

$$D_{fi} = \langle \psi_f | \vec{r} | \psi_i \rangle = \langle \sum_k c_k^f \chi_k | \vec{r} | \sum_s c_s^i \chi_s \rangle = \sum_{ks} c_k^f c_s^i \langle \chi_k | \vec{r} | \chi_s \rangle \tag{13}$$

where the c_k^f and c_s^i are the AO coefficients. The final spectra were calculated by broadening the worked out oscillator strengths (line spectrum) with Gaussian lobes of 850 cm^{-1} half-widths.

4. Results and Discussion

Colors of $Ag^+_xNa^+_{12-x}A$. Silver-containing sodium zeolite A ($Ag^+_xNa^+_{12-x}A$) is colorless in its fully hydrated form, but turns yellow upon dehydration at room temperature under high vacuum. This holds for nearly any exchange degree ($0.13 \leq x \leq 12$). After such activation about 1/3 of the water remains in the cavities, as observed by means of IR spectroscopy.[32] UV/vis spectra of room temperature activated $Ag^+_xNa^+_{12-x}A$ samples are reported in Figure 4. $Na^+_{12}A$ shows no absorption in the whole spectral range investigated. The yellow color of the Ag^+ containing samples is due to the absorption band appearing with a maximum at 25 000 cm^{-1} for $x = 0.5$. It shifts to 22 000 cm^{-1} with increasing x, but no further change is observed for $x > 6$. The presence of this absorption band already at $x < 0.2$ indicates that isolated Ag^+ ions are sufficient to cause it.

Red-colored material was observed upon activation of yellow samples containing more than one Ag^+ per pseudo unit cell at elevated temperature. This is illustrated in Figure 5. We observe that the visible part of the $Ag^+Na^+_{11}A$ spectrum has only slightly changed upon heating. Its color remains yellow. However, the spectra b and c of $Ag^+_6Na^+_6A$ and $Ag^+_{12}A$ show a new band at about 19 000 cm^{-1}. The color of these samples turned from yellow to red. Yellow- and red-colored samples turn colorless again, when exposed to humidity. The reversibility is complete for the yellow ones, as illustrated in Figure 6. However, a broad but weak absorption in the range of 25 000−33 000 cm^{-1} remains after rehydration of the red samples.

These observations strongly indicate that Ag^+ ions coordinated to zeolite oxygen are responsible for the light absorption observed. The spectrum of fully hydrated silver zeolite samples matches that of an aqueous silver perchlorate solution. The band around 45 000 cm^{-1} in Figure 6 is attributed to a charge transfer transition from Ag^+ coordinated water molecules to the empty 5s state of the Ag^+. We write this as $Ag^+(5s) \leftarrow n(H_2O)$ charge transfer transition; see ref 16. In activated silver zeolite materials the Ag^+ is forced to coordinate zeolite oxygen because an insufficient number of water molecules are available. Three different Ag^+ sites were identified based on X-ray experiments, namely Ag^+ at 6- and 8-ring sites, and at 4-ring positions in the sodalite cage.[33] It seems inprobable that the 4-, 6-, and 8-ring oxygens can coordinate Ag^+ in exactly the same way. Differences in the energy levels are therefore to be expected.

$Ag^+_xCa^{2+}_{6-0.5x}A$ and $Ag^+_{9.5}ZK$-4 Zeolites. Additional information concerning this aspect is accessible by considering the site preferences of cations in activated $Na^+_xCa^{2+}_{6-0.5x}A$ mentioned in section 2. The argon adsorption experiments reported in Figure 7 indicate a similar site preference in activated $Ag^+_xCa^{2+}_{6-0.5x}A$ materials and in $Ag^+_{9.5}ZK$-4. We observe that the internal surface of the zeolite is freely accessible by Ar as

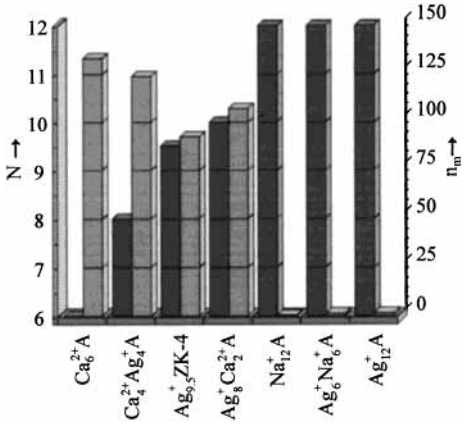

Figure 7. Surface of various cation forms of zeolite A and AgZK-4 measured with Ar at87 K. n_m denotes the monolayer capacity BET in cm^3/g and N the total number of cations per sodalite cage.

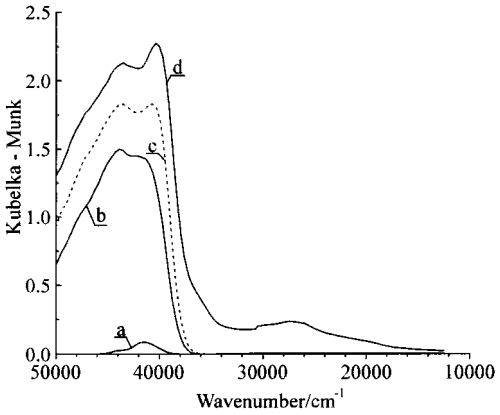

Figure 8. UV/vis spectra of $Ag^+_xCa^{2+}_{6-0.5x}$ A: (a−c) activated at room temperature, (a) $x = 1$; (b) $x = 4$; (c) $x = 5$; (d) activated up to 200 °C, $x = 4$.

long as the total number of cations does not exceed 10. This means that the silver cations prefer 6-ring above 8-ring positions. This allows us to investigate the optical properties of Ag^+ at 6-ring sites. It is safe to assume that in $Ag^+Ca^{2+}_{5.5}A$ the concentration of Ag^+ coordinated to other than 6-ring sites is negligible. On the other hand, we know that in $Ag^+_{10}Ca^{2+}A$ the 6- and the 8-ring positions are highly populated by Ag^+ and that in $Ag^+_{12}A$ at least one 4-ring site is populated.

6-Ring Coordinated Ag^+. Surprisingly, room temperature activated $Ag^+_xCa^{2+}_{6-0.5x}A$ ($x = 1$, 4, and 5) materials are colorless. Their UV/vis spectra are reported in Figure 8. In the sample with the lowest Ag^+ content the $Ag^+(5s) \leftarrow n(H_2O)$ band is missing. Only a weak absorption with a maximum at about 41 000 cm^{-1} can be seen. The absence of the $Ag^+(5s) \leftarrow n(H_2O)$ band means that in this sample the Ca^{2+} ions coordinate the remaining few water molecules so strongly that none of them are left for the Ag^+. The $Ag^+(5s) \leftarrow n(H_2O)$ band reversibly recovers upon rehydration. The Ag^+ can better compete with the Ca^{2+} and capture some water molecules at higher loading. The 41 000 cm^{-1} band becomes much more intense in the $x = 4$ and $x = 5$ samples while the one at 44 000 cm^{-1} is similar as observed in the $Ag^+_xNa^+_{12-x}A$ materials. Upon elevated temperature activation of $Ag^+_4Ca^{2+}_4A$ a new relatively weak broad band appears at about 27 000 cm^{-1}. It cannot be correlated with the intense bands which cause the colors of activated $Ag^+_xNa^+_{12-x}A$. It follows that Ag^+ at 6-ring positions are not the color centers.

6- and 8-Ring Coordinated Ag^+. 8-ring positions are occupied in dehydrated $Ag^+_xCa^{2+}_{6-0.5x}A$ zeolites containing more than 8 ions. We do not know for sure if for $x = 6$ an Ag^+ or a Ca^{2+} is located at the 8-ring position. For $x = 9$, however, at least one Ag^+ has to be there to avoid the less favorable 4-ring sites. We can therefore assume that the spectra of $Ag^+_{10}Ca^{2+}A$ and of $Ag^+_{9.5}ZK\text{-}4$ both reflect cases where several 6-ring positions and at least one 8-ring is occupied by an Ag^+. Both samples are colorless as evident from the UV/vis spectra in Figure 9. However, for $Ag^+_{10}Ca^{2+}A$ we observe a bathochromic shift of the 41 000 cm^{-1} band to 40 000 cm^{-1}. In addition, a new weak band appears at 32 000 cm^{-1}. The 40 000 cm^{-1} band in the spectrum of $Ag^+_{9.5}ZK\text{-}4$ is similar, the 44 500 cm^{-1} band is less intense but no other than that difference can be recognized. The long-wavelength band seems also to build up. From this it is safe to conclude that the influence of Ca^{2+} ions is not responsible for the missing color of room temperature activated $Ag^+_{10}Ca^{2+}A$, because no Ca^{2+} is present in the ZK-4 material.

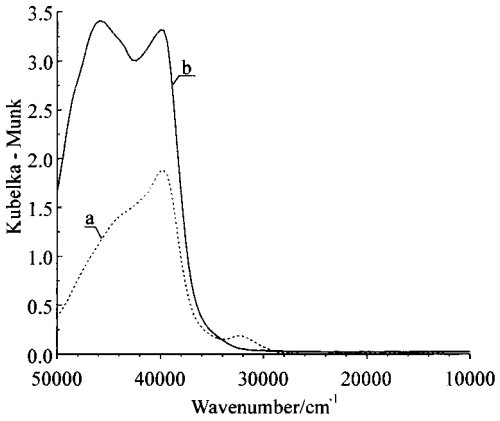

Figure 9. UV/vis spectra of (a) $Ag^+_{10}Ca^{2+}A$ and (b) $Ag^+_{9.5}ZK\text{-}4$, both activated at room temperature.

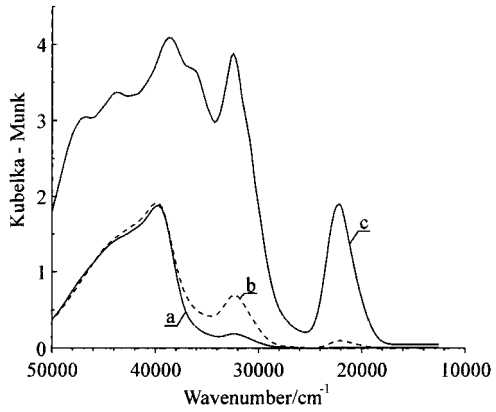

Figure 10. UV/vis spectra of various silver containing zeolites activated at room temperature: (a) $Ag^+_{10}Ca^{2+}A$; (b) $Ag^+_{11}Ca^{2+}_{0.5}A$; (c) $Ag^+_{12}A$.

4-Ring Coordinated Ag^+. Occupation of the 4-rings with Ag^+ ions is expected for $Ag^+_xCa^{2+}_{6-0.5x}A$ materials containing more than 11 Ag^+. It is interesting to observe how this correlates with the development of the yellow color for room temperature activated samples from $Ag^+_{10}Ca^{2+}A$ (a), to $Ag^+_{11}Ca^{2+}_{0.5}A$ (b), to $Ag^+_{12}A$ (c). While (a) is nearly colorless, (b) is slightly yellow, and (c) shows the well-known deep yellow color. This color change can be followed in the spectra in Figure 10. The absorption at 32 000 cm^{-1} already recognized in Figure 9 increases from (a) to (b) and develops into a real strong band in (c). More interestingly, we observe a new weak band in (b) at 22 000 cm^{-1} which becomes intense in the fully exchanged sample (c). This band is responsible for the yellow color. We have encountered it before; see Figures 4 and 6. If activation

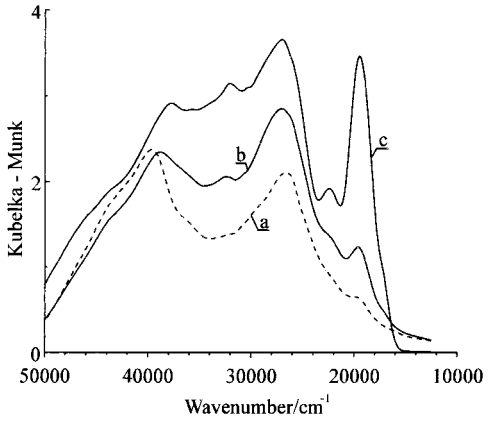

Figure 11. UV/vis spectra of various silver containing zeolites activated up to 200 °C: (a) $Ag^+_{10}Ca^{2+}A$; (b) $Ag^+_{11}Ca^{2+}_{0.5}A$; (c) $Ag^+_{12}A$.

of the $Ag^+_{10}Ca^{2+}A$, $Ag^+_{11}Ca^{2+}_{0.5}A$, and $Ag^+_{12}A$ materials is continued at 200 °C in HV, the spectra shown in Figure 11 evolve. They should be compared to those in Figure 5. We especially recognize the very intense new absorption at about 27 000 cm^{-1} but also the band which starts as a shoulder in (a) and becomes very intense in (c) with a maximum at about 19 000 cm^{-1}. Other $Ag^+_xCa^{2+}_{6-0.5x}A$ with $x < 10$ show a similar behavior as $Ag^+_{10}Ca^{2+}A$, all of them turning slightly brown upon high-temperature activation, while samples with $x > 10$ are dominated by the absorption a 19 000 cm^{-1} which leads to red-colored samples.

Conclusions. Self-synthesized, chemically pure sodium and calcium zeolite A as well as sodium ZK-4 are plain white in both their hydrated and their activated forms. Commercial zeolite A, however, is usually brownish, mostly due to iron as a major impurity, but also chloride is frequently present. All spectra reported in this study are based on chemically pure materials. This means that any absorption band or colors observed are due to the presence of silver ions. The marked site preference of ions in $Ag^+_xCa^{2+}_{6-0.5x}A$, which can be probed by gas adsorption experiments, offers a unique possibility to investigate different coordination sites of Ag^+ ions in zeolite A.

The observations on room temperature activated $Ag^+_xCa^{2+}_{6-0.5x}A$ and $Ag^+_{9.5}ZK\text{-}4$ samples lead to the conclusion that Ag^+ coordinated to 6- and 8-ring oxygens give rise to electronic transition in the range of 39 000−45 000 cm^{-1}. Only 4-ring coordinated Ag^+ leads to an absorption in the visible, namely at 22 000 cm^{-1}, and only these samples show the typical deep yellow color. Since this band is only observed for $x > 10$, we know that Ag^+ avoids the 4-ring site as long as possible. Assuming that the X-ray results of Gellens et al.[33] are valid for the materials investigated by us, we expect that Ag^+ prefers a 4-ring of the sodalite cage above one in α-cage. In $Ag^+_xNa^+_{12-x}A$ either a Na^+ or a Ag^+ is forced to this site, because all other places are occupied. The presence of the 22 000 cm^{-1} absorption band already at $x < 0.2$ proves (i) that isolated Ag^+ ions are sufficient to cause it and (ii) that the Ag^+ coordination to the 4-ring oxygens is significantly stronger than that of the Na^+. We note that the band at about 32 000 cm^{-1} grows parallel to the 22 000 cm^{-1} absorption; see Figures 4 and 10. The 4-ring coordinated Ag^+ are assumed to be responsible for its appearance. To obtain the red color, which is caused by the strong absorption band at 19 000 cm^{-1}, three conditions must be fulfilled: (i) The silver zeolite samples must turn yellow upon activation at room temperature. Samples which remained colorless after room-temperature activation have never been observed to turn red. (ii) More than one Ag^+ per pseudo unit cell must be present. Samples with lower silver content have never been observed to turn red. (iii) The samples must be dehydrated to a great extent which was achieved only upon heating in HV. From this we conclude that only samples with 4-ring coordinated Ag^+ give rise to the 19 000 cm^{-1} band and this only if a second Ag^+ is not too far away. It is the interaction between the two silver species which spawns a lower state giving rise to the red color. We assume that the second Ag^+ is at a 6-ring site because the 8-ring positions are further away. The more complete dehydration is needed in order to enforce this Ag^+-Ag^+ interaction.

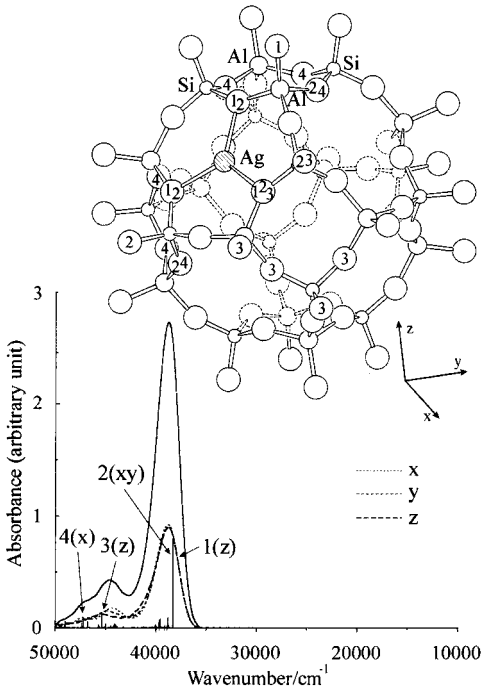

Figure 12. Six-ring coordinated Ag^+: (upper) section of the investigated unit structure cell showing the Ag^+ position at the 6-ring; (lower) calculated electronic transitions (lines) and worked out spectra.

5. Theoretical Considerations

Having identified the color centers of yellow and of red silver zeolite A materials as Ag^+-coordinating zeolite 4-ring oxygens and as Ag^+ at these sites interacting with Ag^+ at 6-ring positions, respectively, we wonder about the nature of the electronic states involved. We report results on 4- and 6-ring sites which were identified by X-ray measurements, namely Ag(1) in front of a 4-ring and Ag(2) at the center of a 6-ring, both located in the sodalite cavity.[33] The position Ag(2′), 0.5 Å displaced from the center of a 6-ring, was found to behave very similarly to Ag(2) and will subsequently be disregarded. We report only results obtained on anhydrous states. The water to silver LMCT transitions were recently described in sufficient detail.[16]

6-Ring Coordinated Ag^+. An Ag^+ at the 6-ring has three nearest-neighbor oxygen atoms at a distance of 2.27 Å to which it is coordinated, as indicated by the three bonds in Figure 12. We show only the atoms of the sodalite cage but not those of the embedding eight α-cages. The numbers 1, 2, 3, and 4 refer to oxygen atoms contributing more than roughly 5% to the initial molecular orbital as determined from a Mulliken population analysis.[34] The letters in parentheses denote the respective polarization of the electronic transitions with respect to the coordinate system we have indicated. The worked out absorption spectrum results from one Ag^+ on a 6-ring. The lines represent the calculated transitions obtained by considering all transitions from the first 1244 levels in the occupied frontier orbital region,

which spreads from −11.08 to −14.01 eV, to the LUMO (−6.34 eV). The LUMO+1 is energetically much up (−3.89 eV) and does therefore not contribute to the spectral range investigated. The smoothed out spectra were obtained by broadening the line spectrum with Gaussian lobes of 850 cm^{-1} half-widths. The solid line represents the sum of the absorption intensities in *x*, *y*, and *z* polarization. The levels in the HOMO region derive from practically noninteracting orbitals with no significant Al or Si mixing; i.e., they are the oxygen lone pairs which we abbreviate as O(n). The LUMO is a rather pure Ag(5s) (58%) with a 30% contribution of the three oxygens to which Ag is bonded. Thus, all electronic excitations in question are ligand-to-metal charge transfer transitions (LMCT) from oxygen lone pairs to the silver ion. They are energetically located in the near-UV and depend only little on the polarization. Two absorption bands appear at roughly 39 000 and 44 500 cm^{-1}, respectively. The first one is mainly made up of three transitions, namely 1(*z*) at 38 270 cm^{-1} ($f_{ed,z} = 0.113$) and the doubly degenerate 2(*xy*) transition at 38 300 cm^{-1} ($f_{ed,x} = 0.096$; $f_{ed,y} = 0.075$). The absorptions contributing most to the high-energy band are 3(*z*) at 45 350 cm^{-1} ($f_{ed,z} = 0.012$) and 4(*x*) at 47 200 cm^{-1} ($f_{ed,x} = 0.012$). These transitions are relatively intense if we compare them with, e.g., the prominent LMCT band responsible for the violet color of the permanganate ion MnO_4^- which bears an oscillator strength of 0.032.[15] We learn, from the positions of the O atoms involved, that the LMCT transitions are restricted neither to the atoms coordinated to the Ag^+ nor to the sodalite cavity. Four (out of five) transitions concern bridging oxygens of double 4-rings. Interestingly, the nearest-neighbor oxygens do not participate in the high-energy absorption 4(*x*), and the other three 6-ring oxygens do not contribute to any of these absorptions for symmetry reasons.

These results can be compared with the experimental spectrum of $Ag^+Ca^+_{5.5}A$ in Figure 8a, where only Ag^+ coordinating at 6-ring positions is present and where the residual water does not disturb. The agreement in shape and position between the computed spectrum and the experiment is certainly decent, given the complexity of the system. The energy of the most intense band is somewhat too low and that of the second one a bit too high. We conclude that a 6-ring coordinated Ag^+ gives rise to transitions from zeolite oxygen lone pairs to the Ag^+ 5s orbital, which we denote as $Ag^+(5s) \leftarrow O(n)$, in the near-UV range.

All 6-Rings Occupied by an Ag^+. At higher Ag^+ content, a broadening of the bands was observed in the experiments reported in Figures 8. To what extent does the interaction between several Ag^+ at 6-ring positions influence the calculated absorption spectrum? We pushed the situation to an extreme and worked out the absorption spectrum for eight silver cations occupying all 6-ring positions. The spectrum (not shown) features three absorption bands at 42 500 cm^{-1} (most intense), 36 000 cm^{-1} (little bit less intense), and at 30 500 cm^{-1} (roughly only one-third of the absorption intensity of the other two bands). The wave functions show that the low-energy band is due to an LMCT transition from the oxygen lone pairs to the silver LUMO, which is an all-bonding linear combination of the eight Ag(5s) orbitals. Given the low statistical probability that Ag^+ occupies exclusively all eight 6-rings of a sodalite cavity in the samples under consideration, it might be difficult to actually observe this band in an experiment. We conclude that broadening and gain in intensity of the absorption bands are expected but that no absorption band in the visible range leading to a colored silver zeolite will be found even on completely occupying all 6-ring positions with Ag^+.

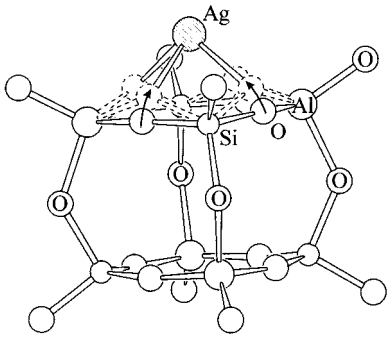

Figure 13. Rearrangement of the 4-ring oxygens on coordinating an Ag^+.

4-Ring Coordinated Ag^+. In order to identify the correct Ag^+-O distances of 4-ring coordinated Ag^+ we face the problem that X-ray diffraction can only accurately reveal atomic positions when the material is sufficiently periodic. In zeolites the cations are not periodically arranged in the crystal, but rather statistically distributed. The anionic framework will locally distort on coordinating these cations. Thus, the positions obtained from X-ray data reflect an averaging over many different situations. The smaller the occupation of a site, the less is its statistical weight and therefore the error in the mutual distances of the respective atoms will increase. This was not a striking problem in the case of the Ag^+ at the 6-ring positions considered in the previous section, with its comparatively high occupancy of 44.2 out of the possible 64 (Wyckoff position 64(g)).[33] Accordingly, the Ag^+-O distance (2.27 Å) agrees well with what one expects for Ag^+ three-coordinated to zeolite oxygen. As a reference we take the Ag^+-O bond lengths for two- (2.15 Å) and four-coordination (2.40 Å). Two-, four-, and six-coordinated complexes are know from crystallographic[35] and EXAFS[36] measurements with linear, tetrahedral, and octahedral geometry, and mean Ag^+-O distances of 2.13, 2.4, and 2.5 Å, respectively. The occupancy of an Ag^+ in front of a 4-ring in the sodalite cavity (Wyckoff position 48(e)), however, was only 5.7 in the crystal investigated by Gellens.[33] The Ag^+ was reported to be four-coordinated to oxygen at an apparent distance of 2.82 Å which is roughly 0.4 Å longer than expected (vide supra). Two explanations are possible: (I) Ag^+ only weakly interacts with the oxygens and finds another way to stabilize itself. (II) The Ag^+-O bond length is actually shorter and the long distance of 2.82 Å is an artifact, resulting from averaging over a set of nonbonding and bonding oxygens, where the former situation dominates. As Ag^+-Ag^+ and Ag^+-Na^+ interactions are clearly repulsive, hypothesis (I) can be excluded. It is well-known from IR and FT-Raman spectroscopy that characteristic $\delta(O-T-O)$ and $\delta(T-O-T)$ bending modes in zeolite A are very soft, the latter coming below 100 cm^{-1} (T = Si, Al).[37] Therefore, it is likely for the oxygens of a 4-ring to bend toward Ag^+ on coordination, leading to a much shorter Ag^+-O distance than the value given above as illustrated in Figure 13. The stabilization due to the increased Ag^+-O interaction compensates for the distortion energy of the 4-ring.

On the basis of this reasoning, we kept the positions of the 4-ring atoms fixed, but placed the Ag^+ at a distance of 2.40 Å from the four oxygens, thus modeling the essence of the Ag^+-O interaction. The resulting density of levels (number of cluster orbitals per 0.001 eV) is shown in the upper panel of Figure 14. The LUMO (visible as a bar of length one) at −8.78 eV is mainly located at Ag^+ (50%) with an 11% contribution from each of the four bonding oxygens. The one-sided coordination of Ag^+ results in a significant s−p mixing of the respective orbitals (70% 5s; 30% $5p_z$). This is in contrast to the planar

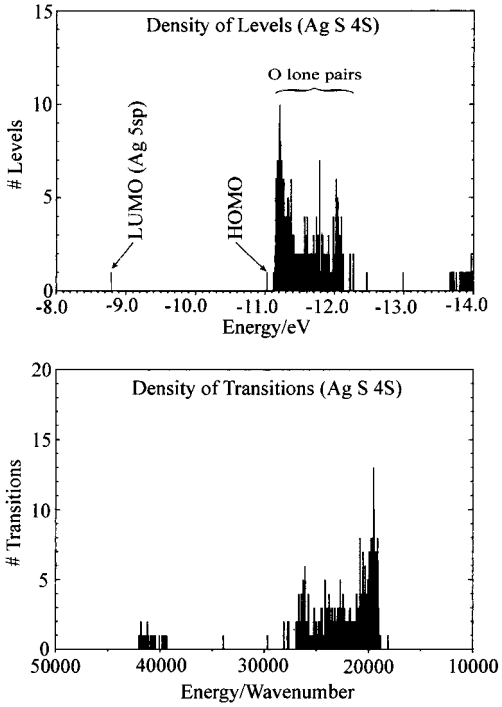

Figure 14. Four-ring coordinated Ag^+ in the sodalite cage: (upper) density of levels (DOL); (lower) density of transitions (DOT).

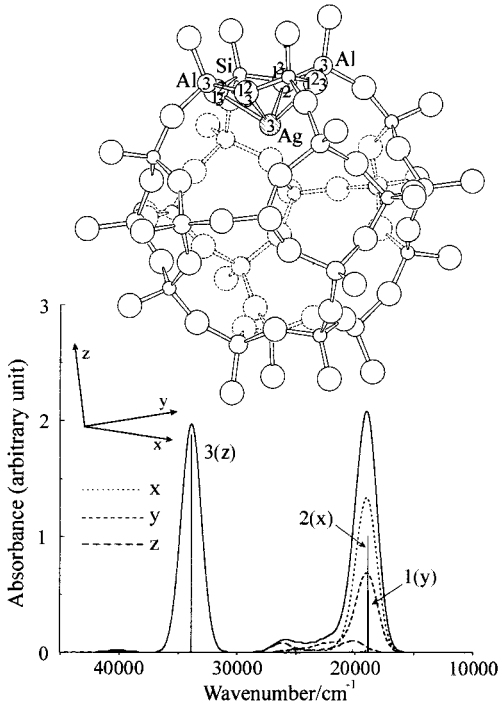

Figure 15. Four-ring coordinated Ag^+: (upper) section of the investigated unit structure cell showing the Ag^+ position at the 4-ring; (lower) calculated electronic transitions (lines) and worked out spectra.

3-fold coordination at the center of a 6-ring where the Ag^+ contributes an almost pure 5s orbital to the LUMO. The HOMO at −11.03 eV is to 82% composed of oxygen $2(p_x,p_y,p_z)$ orbitals hybridized such as to point to Ag^+ and slightly interacting with its $5d_{xy}$ orbital. (For the orientation of the coordinate system see inset in Figure 15). A small energy gap of 0.1 eV separates the HOMO from the oxygen lone pairs. The first 1244 levels in the frontier orbital region ranging from −11.03 to −13.99 eV were used to work out the density of transitions (DOT) and the oscillator strengths for the electronic absorptions to the LUMO. The superjacent LUMO+1 is again high in energy (−3.60 eV) and may be disregarded for the same reason as before. The DOT (number of transitions in an energy window of 10 cm^{-1}) is shown in the lower panel of Figure 14. It looks like the mirror image of the DOL, which is easy to understand as in the present case we consider electronic transitions to one single final level. (Needless to say, had we to take into account more levels in the LUMO region, the complexity of the DOT would swiftly increase.) Densities of transitions are sometimes used to estimate electronic absorption spectra, especially in solid state physics.[38] Even though DOT plots may provide useful information regarding the features of electronic absorption spectra, the actual spectra are revealed only after weighting the DOT with the corresponding absorption probabilities (i.e., oscillator strengths); see also ref 17. It is remarkable that out of the 1244 transitions, only three significantly contribute to the line spectrum which we report in Figure 15. They are 1(*y*), 2(*x*), and 3(*z*). The comparably high DOT grouped around 40 000 cm^{-1} has no effect on the absorption spectrum whereas the single transition at 33 900 cm^{-1} accounts for the whole high-energy absorption band.

Figure 15 is organized similarly to Figure 12. In contrast to the 6-ring case we recognize a pronounced polarization dependence of the bands. The low-energy absorption at 19 000 cm^{-1} is mainly *xy*-polarized and consists of the transitions 1(*y*) at 18 846 cm^{-1} from the HOMO-1 to the LUMO ($f_y = 0.112$) and 2(*x*) at 18 899 cm^{-1} from the HOMO-2 to the LUMO ($f_x = 0.219$). Both transitions are almost degenerate, but differ in intensity due to the absorption along the Si−Si direction of the 4-ring. The high-energy band at 33 900 cm^{-1} is fully *z*-polarized ($f_z = 0.421$). Not only do both of these bands differ regarding their polarization, but also regarding their type. The first (low-energy) band can be described as an LMCT transition from oxygen-centered orbitals to silver $Ag^+(5s) \leftarrow O(n)$. However, the near UV band exhibits a significant $Ag^+(5s) \leftarrow \sigma$ character as found from the 30% silver contribution to the respective initial wave function. 4-ring coordinated Ag^+ is present in room-temperature activated $Ag^+_xNa^+_{12-x}A$. We therefore compare the computational results with the spectrum reported in Figure 4. The experimentally observed high-energy region is a superposition of the water to silver LMCT transitions and of transitions caused by Ag^+ coordinated to zeolite oxygens. The intense HOMO/LUMO $Ag^+(5s) \leftarrow O(n)$ transition, polarized in *x* and *y* directions, correlates with the intense 22 000 cm^{-1} absorption responsible for the yellow color of these samples, regardless of the fact that its energy is somewhat underestimated. It seems natural to assigne the $Ag^+(5s) \leftarrow \sigma$ transition to the 32 000 cm^{-1} band which we observed to grow together with the first $Ag^+(5s) \leftarrow O(n)$ transition. We conclude that the HOMO/LUMO $Ag^+(5s) \leftarrow O(n)$ transition of 4-ring coordinated Ag^+ is in agreement with the appearance of a deep yellow color of room-temperature activated Ag^+-exchanged zeolite A materials with occupied 4-ring positions in the sodalite cavity.

6. Conclusions

We studied the UV/vis spectra of $Ag^+_xNa^+_{12-x}A$ and of $Ag^+_xCa^{2+}_{6-0.5x}A$ materials in their fully hydrated, in HV room temperature dehydrated, and in HV elevated temperature dehydrated states. The marked site preference of the ions in $Ag^+_xCa^{2+}_{6-0.5x}A$, probed by gas adsorption experiments, offered the unique possibility of investigating different coordination sites of Ag^+ ions in zeolite A. Pure sodium and calcium zeolite A are colorless in both their hydrated and their activated states. They do not absorb light within the spectral range from 50 000

to 10 000 cm^{-1} we have investigated. This means that any absorption band or colors observed in silver zeolite A materials are due to the presence of silver ions.

We found that 6- and 8-ring coordinated Ag^+ gives rise to electronic transitions in the near-UV region. An absorption in the visible, namely at 22 000 cm^{-1}, was only observed in materials where 4-ring coordinated Ag^+ was present and only they showed the typical deep yellow color. We also observed that Ag^+ avoids the 4-ring sites as long as possible in $Ag^+_xCa^{2+}_{6-0.5x}A$, namely as long as x is smaller than 10. In the case of $Ag^+_xNa^+_{12-x}A$, either a Na^+ or a Ag^+ is forced to coordinate a 4-ring site because all other places are occupied. The presence of the 22 000 cm^{-1} absorption responsible for the yellow color, already at $x < 0.2$, proves that isolated Ag^+ ions are sufficient to cause it and that the 4-ring coordination of Ag^+ is significantly stronger than that of the Na^+. The red color of elevated temperature activated samples is caused by a strong absorption band at 19 000 cm^{-1}. We observed that samples which remained colorless after room temperature activation never turned red, that samples with lower silver content than one Ag^+ per pseudo unit cell never turn red, and that room temperature dehydration under our experimental conditions was not sufficient to produce red colored samples. These observations strongly indicate that only samples with 4-ring coordinated Ag^+ can give rise to the 19 000 cm^{-1} band and this only if a second Ag^+ is not too far away at a 6-ring site, so that they can interact to develop a corresponding low-lying state.

Molecular orbital calculations carried out on a sufficiently large zeolite part, obtained by fusing eight α-cages at 8-rings, which leads to the unit cell of zeolite A shown in Figure 1c, allowed us to address questions about the nature of the HOMO and of the LUMO region, about the contributions of the zeolite framework atoms to the electronic transitions, about the influence of the local symmetry of the Ag^+ at 4- and at 6-ring sites and about the importance of Ag^+-Ag^+ interactions. In order to avoid geometries without experimental relevance, we restricted this study to Ag^+ at 4- and 6-ring sites known from X-ray measurements.

The occupied frontier orbital region consists manly of two bunches of levels: the HOMO region from about −11 to −12.6 eV and the next levels below −13.6 eV. The LUMO consists of a single level of mainly $Ag^+(5s)$ character. The LUMO+1 was found to be energetically too high to be of relevance in this study. Thus, the oscillator strength of transitions from the first 1244 levels to the LUMO were calculated. For 6-ring coordinated Ag^+ all levels in the HOMO region derive from mostly noninteracting oxygen lone pairs which we abbreviate as O(n). The LUMO is a rather pure Ag(5s) with some contribution from the three coordinating oxygens. Thus, all electronic excitations in question are ligand-to-metal charge-transfer transitions (LMCT) from oxygen lone pairs to the silver ion. They are energetically located in the near-UV and depend only little on the polarization. The agreement in shape and position between the computed spectrum and the experiment allowed us to conclude that a 6-ring coordinated Ag^+ gives rise to electronic transitions from zeolite oxygen lone pairs to the Ag^+ 5s orbital in the near-UV. We denote such electronic transitions as $Ag^+(5s) \leftarrow O(n)$. The bands of the 4-ring coordinated Ag^+ are strongly polarized. Two almost degenerate low-energy absorption bands and a prominent high-energy band dominate the spectrum. Not only do both of these bands differ regarding their polarization, but also regarding their type. The first one can be described as an $Ag^+(5s) \leftarrow O(n)$ LMCT transition. It is responsible for the yellow color. The near-UV band exhibits a significant $Ag^+(5s) \leftarrow \sigma$ character. It is natural to assign it to the 32 000 cm^{-1} band. Interestingly, out of the 1244 electronic transitions from the frontier orbital region to the LUMO, only three bear significant intensity (see Figures 14 and 15). This clearly demonstrates the paramount importance of oscillator strengths and how problematic an estimation of electronic spectra based on DOL arguments alone can be. We conclude that the calculated $Ag^+(5s) \leftarrow O(n)$ transition of 4-ring coordinated Ag^+ is in agreement with the appearance of a deep yellow color of room temperature activated Ag^+-containing zeolite A materials with occupied 4-ring positions in the sodalite cavity.

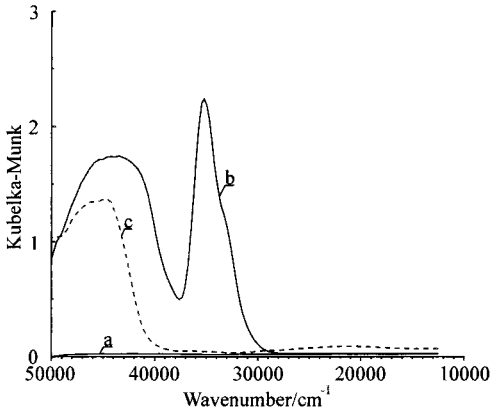

Figure 16. UV/vis spectra of zeolite Y: (a) $Na^+_{69}Y$, (b) $Ag^+_{69}Y$, activated at room temperature, (c) the same as (b) but after exposure to moisture.

6-Ring coordinated Ag^+ give rise to electronic transitions in the near-UV and 4-ring coordinated Ag^+ is responsible for the deep yellow color of the room-temperature activated material. This implies that similar $Ag^+(5s) \leftarrow O(n)$ LMCT transitions are to be expected in other Ag^+-exchanged zeolites. Ag^+-exchanged zeolite Y can be used as a test. We therefore report in Figure 16 UV/vis spectra of (a) pure $Na^+_{69}Y$, (b) room temperature HV dehydrated $Ag^+_{69}Y$, and (c) the same as (b) after exposure to moisture. The main result is that an intense band at about 34 000 cm^{-1} appears upon dehydration which vanishes upon rehydration. By analogy, one would also expect a similar type of LMCT transitions in Cu^+ zeolite materials. $Cu^+(4s) \leftarrow O(n)$ LMCT transitions, reversible upon HV hydration/dehydration, have indeed been observed in Cu^+ zeolit A und X.[39,40]

Lastly, it is obvious that our results are in contradiction to the autoreduction process which was postulated to be the reason for the color changes of silver zeolite A,[2] first observed by Rálek et al. in 1962.[1]

Acknowledgment. This work was supported by the Swiss National Science Foundation, project NF 2000-053414/98/1, and by the Schweizerische Bundesamt für Energie BFE, project no. 10441. We thank David Schürch for carefully reading the manuscript.

References and Notes

(1) Rálek, M.; Jíru, P.; Grubner, O.; Beyer, H. *Collect. Czech. Chem. Commun.* **1962**, *27*, 142.

(2) Sun, T.; Seff, K. *Chem. Rev.* **1994**, *94*, 857.

(3) Seifert, R.; Kunzmann, A.; Calzaferri, G. *Angew. Chem., Int. Ed. Engl.* **1998**, *37* (11), 1521.

(4) Smart, L.; Moore, E. *Solid State Chemistry*; Chapman & Hall: London, 1995.

(5) Meier, W. M.; Olson, D. H.; Baerlocher Ch. *Atlas of Zeolite Structure Types;* Elsevier: London, 1996.

(6) Breck, D. W.; Eversole, W. G.; Milton, R. M.; Reed, T. B.; Thomas, T. L. *J. Am. Chem. Soc.* **1956**, *78*, 5963.
(7) Reed, T. B.; Breck, D. W. *J. Am. Chem. Soc.* **1956**, *78*, 5972.
(8) Kerr, G. T. *Inorg. Chem.* **1966**, *9*, 1537.
(9) Loewenstein, W. *Am. Mineral.* **1954**, *39*, 92.
(10) Pluth, J. J.; Smith, J. V. *J. Am. Chem. Soc.* **1983**, *105*, 2621.
(11) Pluth, J. J.; Smith J. V.; *J. Am. Chem. Soc.* **1980**, *102*, 4704.
(12) Kosslick H.; Roethe, A.; Roethe K.-P. *Chem. Technik* **1994**, *46*, 101.
(13) Breck, D. W. *Zeolite Molecular Sieves*; John Wiley: New York, 1974.
(14) Ruthven, D. M. *Can. J. Chem.* **1974**, *52*, 3523.
(15) Calzaferri, G.; Rytz, R. *J. Phys. Chem.* **1995**, *99*, 12141.
(16) Glaus, S.; Calzaferri G. *J. Phys. Chem. B* **1999**, *103*, 5622.
(17) Rytz, R.; Calzaferri, G. *J. Phys. Chem. B* **1997**, *101*, 5664.
(18) Feynman, R. P.; Leighton, R. B.; Sands, M. *The Feynman Lectures on Physics*; Addison-Wesley: Reading MA, 1966.
(19) Lainé, P.; Seifert, R.; Calzaferri, G. *New. J. Chem.* **1997**, *21*, 453.
(20) Li, J. W.; Pfanner, K.; Calzaferri, G. *J. Phys. Chem.* **1995**, *99*, 2119.
(21) Sherry, H. S.; Walton, H. F. *J. Phys. Chem.* **1967**, *71*, 1457.
(22) Hoffmann, R. *J. Chem. Phys.* **1963**, *39*, 1397.
(23) Rytz, R.; Glaus, S.; Brändle, M.; Brühwiler, D.; Calzaferri, G. *ICON-EDiT, Extended Hückel Molecular Orbital and Transition Dipole Moment Calculations*; URL: http://iacrs1.unibe.ch/; Department of Chemistry and Biochemistry, University of Berne, Freiestrasse 3, 3012 Bern, Switzerland, 1997, update 1999.
(24) Wolfsberg, M.; Helmholz, L. *J. Chem. Phys.* **1952**, *20*, 837.
(25) Ammeter, J. H.; Bürgi, H.-B.; Thibeault, J. C.; Hoffmann, R. *J. Am. Chem. Soc.* **1978**, *100*, 3686.
(26) Brühwiler, D.; Gfeller, N.; Calzaferri, G. *J. Phys. Chem. B* **1998**, *102*, 2923.
(27) Basch, H.; Viste, A.; Gray, H. B. *Theor. Chim. Acta* **1965**, *3*, 458.
(28) McGlynn, S. P.; Vanquickenborne, L. G.; Kinoshita, M.; Carroll, D. G. *Introduction to Applied Quantum Chemistry*; Holt, Rinehart and Winston Inc.: New York, 1972.
(29) Rytz, R. Dissertation, University of Bern, 1997.
(30) Hoffmann, R. *A Chemist's View of Bonding in Extended Structures*; VCH: Weinheim, Germany, 1988.
(31) Kuhn, H. *J. Chem. Phys.* **1958**, *29*, 958.
(32) Seifert, R. Dissertation, University of Bern, 1999.
(33) Gellens, L. R.; Smith, J. V.; Pluth, J. J. *J. Am. Chem. Soc.* **1983**, *105*, 51.
(34) Mulliken, R. S. *J. Chem. Phys.* **1955**, *23*, 1833.
(35) Yamaguchi, T.; Johansson, G.; Holmberg, B.; Maeda, M.; Othaki, H. *Acta Chem. Scand. A* **1984**, *38*, 437.
(36) Tsutsui, Y.; Sugimoto, K.; Wasada, H.; Inada, I.; Funahashi, S. *J. Phys. Chem. A* **1997**, *101*, 2900.
(37) Bärtsch, M.; Bornhauser, P.; Calzaferri, G.; Imhof, R. *J. Phys Chem.* **1994**, *98*, 2817.
(38) Knox, R. S. *Theory of Excitons*; Academic Press: New York, 1963.
(39) Beer, R.; Calzaferri, G.; Kamber, I. *J. Chem. Soc., Chem. Commun.* **1991**, 1489.
(40) Calzaferri, G.; Giovanoli, R.; Kamber, I.; Shklover, V.; Nesper, R. *Res. Chem. Intermed.* **1993**, *19*, 31.